

# Experimental and theoretical study on elastic properties of crystalline alkali silicate hydrate

Juhyuk Moon <sup>a, b</sup>, Seungchan Kim <sup>a</sup>, Cagla Meral Akgul <sup>c</sup>, Sung-Chul Bae <sup>d, \*</sup>, Simon Martin Clark <sup>e</sup>

<sup>a</sup> Department of Civil and Environmental Engineering, Seoul National University, Seoul, 08826, Republic of Korea

<sup>b</sup> Institute of Construction and Environmental Engineering, Seoul, 08826, Republic of Korea

<sup>c</sup> Department of Civil Engineering, Middle East Technical University, Ankara, 06800, Turkey

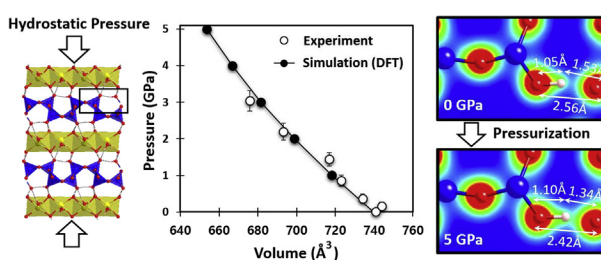
<sup>d</sup> Department of Architectural Engineering, Hanyang University, Seoul, 04763, Republic of Korea

<sup>e</sup> Department of Earth and Planetary Sciences, Macquarie University, North Ryde, NSW, 2019, Australia

## HIGHLIGHTS

- Synthesized Na-kanemite,  $\text{NaH-Si}_2\text{O}_5 \cdot 3(\text{H}_2\text{O})$  showed reversible pressure instability.
- Under pressure of 0.4 GPa, a new 011 peak formed while 020 interlayer peak was diffused due to the reduction of  $Pbcn$  symmetry.
- Based on the good agreement between experiment and density functional theory based calculation, reliable elastic coefficients at low pressure have been proposed.
- Applied pressure was dominantly absorbed by the space between silicate and Na layer.

## GRAPHICAL ABSTRACT



## ARTICLE INFO

### Article history:

Received 25 June 2019

Received in revised form

4 September 2019

Accepted 25 September 2019

Available online 7 October 2019

### Keywords:

Na-kanemite

High pressure x-ray diffraction

Density functional theory

First-principles calculation

Mechanical properties

Elastic coefficients

## ABSTRACT

Mechanical properties of synthesized sodium silicate mineral, Na-kanemite, was investigated by synchrotron-based high-pressure x-ray diffraction experiment and first-principles calculations. Under hydrostatic pressure, the 020 interlayer peak was substantially diffused while a new 011 peak formed at 0.4 GPa due to the reduction of  $Pbcn$  symmetry. Upon unloading, the diffused interlayer peak reappeared to its original position with a less peak intensity and the newly formed peak disappeared. This temporal but reversible phase instability related to the symmetry reduction, can be induced from the vibration effect of water molecules contained in interlayer region that can more significantly affect the structural response of crystals with poor crystallinity and stacking disorder. There is a good agreement of pressure response between experimental data and calculations using GGA functional. In addition, conducted analysis on bond variation revealed that contraction of thickness and distortion of Na layer under pressure which caused partial charge redistribution. Suggested elastic properties and charge data will be used to develop reliable force-field database for further molecular dynamics simulation and diagnose macroscopic impact from alkali-silicate reaction damaged structure.

© 2019 The Authors. Published by Elsevier Ltd. This is an open access article under the CC BY-NC-ND license (<http://creativecommons.org/licenses/by-nc-nd/4.0/>).

\* Corresponding author.

E-mail address: [sbae@hanyang.ac.kr](mailto:sbae@hanyang.ac.kr) (S.-C. Bae).

## 1. Introduction

Layered microporous hydrous silicates are of industrial and scientific interests due to their role as precursor materials, ion exchanger for waste solidification, or storage for radioactive materials [1–3]. Kanemite crystal was first synthesized by Kalt and Wey and later found at Lake Chad [4,5]. Similar to other layered sodium silicate hydrates such as makatite, octosilicate, magadiite, and kenyaite, its structure has  $\text{Na}_2\text{O} \cdot (4-22)\text{SiO}_2 \cdot (5-19)\text{H}_2\text{O}$  framework. Particularly, the crystal structure of Na-kanemite was known to have isostructural relation to the anhydrous mineral such as  $\text{Ba}_2\text{Si}_4\text{O}_{10}$  or  $\text{KHSi}_2\text{O}_5$  [6]. Almond et al. performed  $^{29}\text{Si}$ ,  $^1\text{H}$  and  $^{23}\text{Na}$  NMR studies to reveal that the crystal structure of kanemite is based on the structure of the anhydrous silicate,  $\text{KHSi}_2\text{O}_5$  [7]. In addition, Hayashi studied detailed dynamics of interlayer cations and water in kanemite [8]. Subsequently, Vortmann et al. resolved the crystal structure by x-ray power diffraction with the Rietveld analysis [9]. They compared the structure of kanemite with sanbornite and synthetic  $\text{KHSi}_2\text{O}_5$  and suggests that it has the interlayer charge balancing cations of Na and H. This result was reinforced by single-crystal x-ray diffraction study. Garvie et al. revealed detail arrangements of atoms consisting of alternating sheets of corrugated silicate sheet and hydrated Na and their hydrogen bonding scheme as shown in Fig. 1 [10].

Along with other layered hydrous silicates, the layered sodium silicate hydrates have common physical properties such as a high capacity for ion exchange by replacing sodium ions with protons or Al. Therefore, they are useful in catalyst or detergent applications [7,11]. Furthermore, the mineral of Na-kanemite is also of interest in cement chemistry society due to the crystallographic similarity with alkali-silica reaction (ASR) gel [12,13]. Although there have

been in-depth studies on structural investigation of the kanemite crystal, its structural responses under pressure is yet to be revealed. Furthermore, due to the structural similarity with ASR gel, the response of Na-kanemite under pressure is critical to understand the impact of expansive nature of the alkali-silica reaction and design more durable infrastructure considering the potential risk of ASR formation. For instance, mechanical properties of this phase can be used in a homogenization scheme to estimate the macro-scale mechanical behavior of ASR damaged structure. Furthermore, considering a wide range of potential applications of kanemite such as catalyst, its thermodynamic stability can be understood by calculating structural response of the crystal under various situations.

High-pressure x-ray diffraction (HPXRD) technique provides valuable experimental data to compute intrinsic mechanical properties of crystalline minerals. Recently, significant understanding on structural responses of calcium aluminate hydrates and calcium silicate hydrates have been achieved from the use of synchrotron x-ray radiation [14–17]. Furthermore, the experimental investigation of atomistic deviation under various conditions can be directly combined with molecular modeling [15,18,19]. The molecular modeling is also an effective tool for studying the structure of crystals at the molecular level and predicting various properties of materials, and is useful when used in conjunction with available experimental data such as HPXRD. In this study, structural responses of synthesized Na-kanemite was investigated by HPXRD experiments. The variations of lattice parameters and volumes under pressure were refined. As a benchmark to the experimental data, first-principles calculations using different exchange-correlation functionals were performed to support the experimental results, propose reliable elastic coefficients, and further elucidate the pressure absorption mechanism.

## 2. Synchrotron based high-pressure X-ray diffraction

### 2.1. Material synthesis

The Na-kanemite tested for a HPXRD experiment was synthesized through a sol-gel method [20]. The synthesis process selected in current study is as follows: (1) In a Teflon beaker, 1 mol of fine silica powder was dispersed in methanol solution. (2) 1 mol of NaOH solution was added to the silica suspended methanol solution for obtaining a 1:1  $\text{SiO}_2$ –NaOH mixture. These processes were conducted under  $\text{CO}_2$  free environment. (3) The resulting gel-like slurry was dried for 3 h in an oven heated at  $100^\circ\text{C}$ . (4) Obtained material was ground and calcined for 5–6 h at  $700^\circ\text{C}$ . (5) After cooling to room temperature, the calcined solid was pulverized using a mortar and pestle. (6) Lastly, the fine powder was dispersed in water, stirred for 15 min, filtered out and air-dried. The obtained Na-kanemite has 23.3 wt% water content that was confirmed by thermal gravimetric analysis (TGA). As presented in the bottom of Fig. 2, its x-ray diffraction (XRD) pattern agrees well with that of the known structure of Na-kanemite,  $\text{NaHSi}_2\text{O}_5 \cdot 3(\text{H}_2\text{O})$  [9].

### 2.2. Experimental procedure and analysis

Using a synchrotron monochromatic x-ray, ambient and high pressure x-ray diffraction experiments were performed in the beamline 12.2.2 of the Advanced Light Source [21]. The sample-to-detector distance of 442 mm and x-ray wavelength of  $\lambda = 0.6199 \text{ \AA}$  were selected for both the ambient and high-pressure experiments. A symmetric diamond anvil cell (DAC) was used to generate a hydrostatic pressure during the expose of x-ray. Powder form of Na-kanemite sample was finely ground and mixed with a few ruby chips whose fluorescence was measured for accurate calibration of

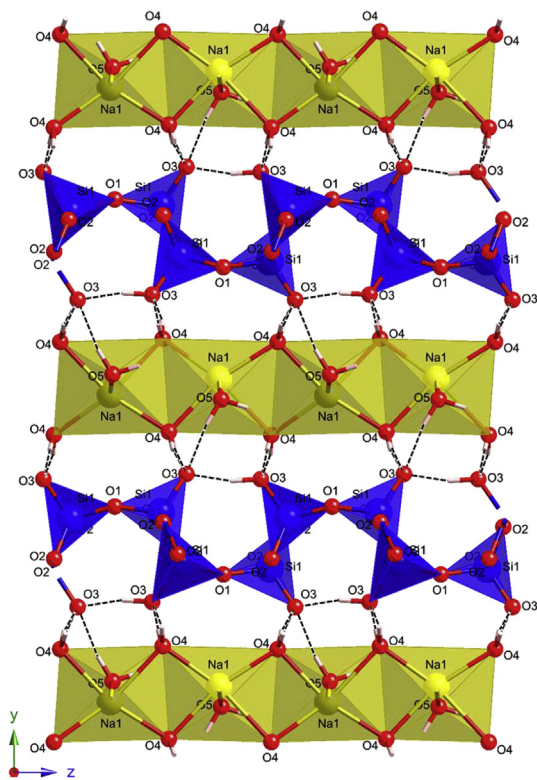


**Fig. 1.** Crystal structure of Na-kanemite projected along [100]. The yellow and blue layers indicate the  $\text{NaO}_6$  octahedra and  $\text{SiO}_4$  tetrahedra, respectively. Red, blue, and yellow spheres represent O, Si, and Na, respectively. Hydroxyl groups and hydrogen atoms in water are denoted with dot sticks.

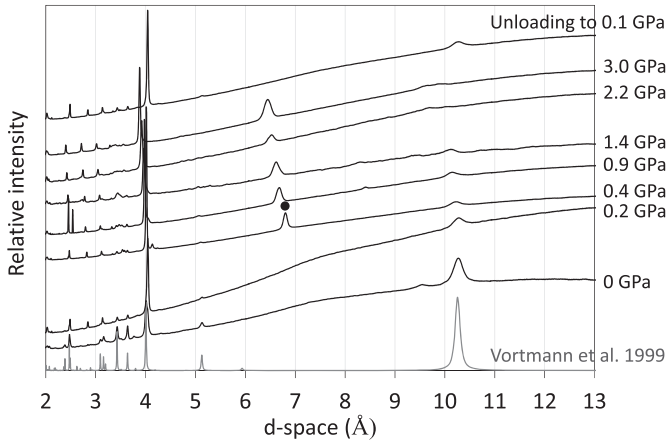


**Fig. 2.** Integrated powder XRD patterns, where the pattern with 0 GPa was measured at ambient condition and the others were measured through DAC containing silicone oil. New peak (●), 011 Bragg peak, appears at 0.4 GPa due to the reduction of *Pbcn* symmetry and disappears when unloading to 0.1 GPa. Bottom peaks indicate reference peak positions from Vortmann et al. [7].

internal pressure in the DAC [22]. For the pressure calibration, three measurements were made before and after an XRD experiment, respectively. Then, averaged data with obtained standard deviation was used to estimate the internal pressure state inside the DAC during each HPXRD experiment. A pressure-transmitting medium of silicone oil (a mixture of polysiloxane chains with methyl and phenyl groups) was filled in the hole inside the DAC. X-ray exposing times of 180 s and 600 s were selected to get adequate intensity of reflections of ambient condition and high-pressure with the DAC experiments, respectively.

For the refinement of lattice parameters, XRD reflections of 020, 040, 031, 200, 220, 051, 002, and 301 were selected. Collected two-dimensional patterns were radially integrated using the Fit2D software to construct plots of d-spacing vs. diffracted intensity [23]. The Integrated XRD patterns are shown in Fig. 2. Then, the accurate positions of peak reflections were determined using the XFIT software and lattice parameters were refined using the CELREF software [24]. Refined lattice parameters at different pressures were summarized in Figs. 2–6 and Table 1.

The measured ambient XRD pattern is in a good agreement with that of S. Vortmann et al. [9]. The strong peak at 4 Å is due to the peaks from ruby chips and stainless steel gasket of the DAC. To compute its bulk modulus, the equation of Birch-Murnaghan Equation of State (BM EoS) was fitted to pressure-volume data points in Eqn. (1) [25].

$$P = 1.5K_0 \left[ (V_0/V)^{7/3} - (V_0/V)^{5/3} \right] \left[ 1 + 0.75(K'_0 - 4) \left\{ (V_0/V)^{2/3} - 1 \right\} \right] \quad (1)$$

where  $V$  is the volume of refined unit cell,  $V_0$  is the volume at zero pressure,  $P$  is the pressure applied to the sample,  $K_0$  is the isothermal bulk modulus at zero pressure, and  $K'_0$  is the first derivative of the bulk modulus at zero pressure. Since the number of measured data points is small,  $K'_0$  was fixed to 4 [25]. Then a weighted linear least-squares fitting gives the bulk modulus of  $K_0 = 30 \pm 4$  GPa with a fitting convergence of  $R^2 = 0.96$  (Fig. 6).

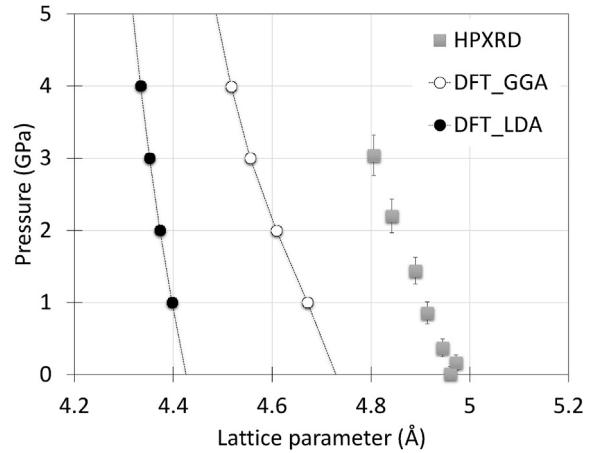


**Fig. 3.** Pressure behavior of lattice parameter  $a$ . Rectangular and circular points (open-GGA and closed-LDA) indicate HPXRD measurement and DFT calculations, respectively.

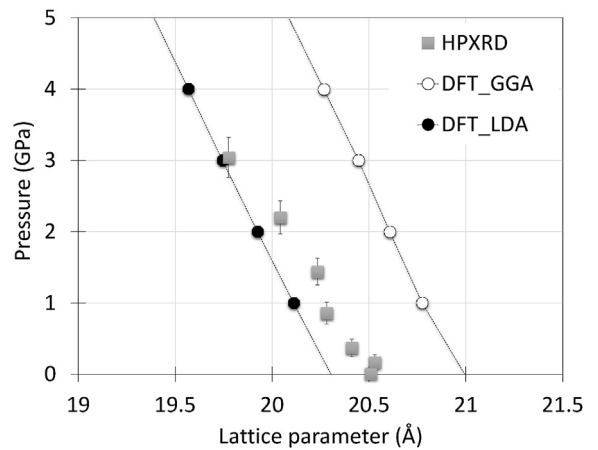


**Fig. 4.** Pressure behavior of lattice parameter  $b$ . Rectangular and circular points (open-GGA and closed-LDA) indicate HPXRD measurement and DFT calculations, respectively.

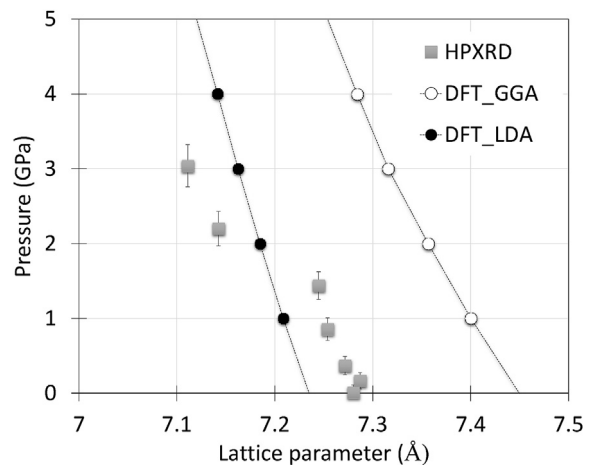


**Fig. 5.** Pressure behavior of lattice parameter  $c$ . Rectangular and circular points (open-GGA and closed-LDA) indicate HPXRD measurement and DFT calculations, respectively.

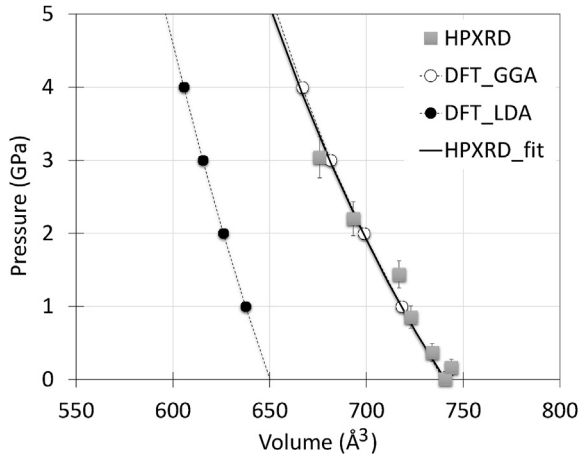


**Fig. 6.** Volumetric behavior under pressure. Rectangular and circular points (open-GGA and closed-LDA) indicate HPXRD measurement and DFT calculations, respectively. Solid line shows 2nd order BM EoS fitting result with an isothermal bulk modulus of 30.2 GPa.

**Table 1**  
Refined lattice parameters and resulting unit-cell volume from a high-pressure x-ray diffraction experiment.

P (GPa)	a (Å)	b (Å)	c (Å)	V (Å <sup>3</sup> )
Ambient	4.961 (4)	20.51 (1)	7.280 (5)	740.6 (9)
0.2 (1)	4.972 (2)	20.53 (1)	7.287 (2)	743.8 (5)
0.4 (1)	4.945 (1)	20.41 (1)	7.272 (2)	733.9 (4)
0.9 (2)	4.914 (1)	20.28 (7)	7.254 (2)	722.9 (3)
1.4 (2)	4.890 (1)	20.23 (7)	7.245 (2)	716.8 (3)
2.2 (2)	4.842 (2)	20.04 (2)	7.143 (4)	693.2 (8)
3.0 (3)	4.806 (8)	19.78 (1)	7.111 (2)	675.8 (4)

Note: Standard deviations in parentheses.

### 3. First-principles calculations

#### 3.1. Computational details

This section describes computational details to simulate structural responses of Na-kanemite. The initial crystal structure used for the simulation has an orthorhombic symmetry ( $a = 4.946$  Å,  $b = 20.510$  Å, and  $c = 7.277$ ) with a space group of  $Pbcn$  as determined by XRD, previously [9]. The missing hydrogen atoms from the XRD experiment were arbitrarily positioned and the hydrogen bonding scheme was later optimized. The DFT calculations were performed using Local-Density-Approximation (LDA) and Perdew-Burke-Ernzerhof (PBE) Generalized-Gradient-Approximation (GGA) exchange-correlation functionals and plane wave techniques implemented in the Quantum ESPRESSO distribution [26]. Ultrasoft type exchange-correlation functionals were used with a plane-wave energy cut-off of 640 eV and a  $\gamma$ -point sampling [27]. Before calculating the structural properties, geometrical optimizations were performed at zero pressure. Lattice parameters and fractional atomic positions were iteratively changed until computed forces were smaller than  $10^{-4}$  eV/Å and total energy difference was less than  $10^{-6}$  eV. The residual stress components of the optimized structure were less than 0.1 kbar. Likewise, equilibrium structures at different pressures (1.0, 2.0, 3.0, 4.0, and 5.0 GPa) were obtained using damped variable cell shape molecular dynamics [28]. Resulting lattice parameters at different pressures using LDA and GGA are presented in Table 2 and Figs. 3–6.

**Table 2**  
Predicted lattice parameters and unit-cell volumes from first-principles calculations.

	P (GPa)	a (Å)	b (Å)	c (Å)	V (Å <sup>3</sup> )
DFT_GGA	0.00	4.73	20.99	7.45	739.69
	1.00	4.67	20.77	7.40	718.16
	2.00	4.61	20.61	7.36	698.70
	3.00	4.56	20.45	7.32	681.42
	4.00	4.52	20.27	7.28	666.86
DFT_LDA	5.00	4.49	20.09	7.25	653.72
	0.00	4.43	20.30	7.24	650.21
	1.00	4.40	20.11	7.21	637.52
	2.00	4.37	19.92	7.18	626.01
	3.00	4.35	19.74	7.16	615.42
	4.00	4.33	19.57	7.14	605.59
	5.00	4.32	19.39	7.12	596.20

#### 3.2. Computational results

For infinitesimal strains, a stress-strain relation is linear that allows to calculate elastic coefficients.

$$\sigma_i = \sum_{j=1}^6 C_{ij} \varepsilon_j \quad (2)$$

Individual strains were applied to the structure optimized at 0 GPa. Then, internal degrees of freedom of all atoms were optimized again. Resulting residual stress components on the re-optimized structures were less than 0.1 kbar. Below Lagrangian strains in Cartesian coordinates were applied to compute the nine independent elastic coefficients:

$$\varepsilon_6 = \begin{pmatrix} 0 & \delta/2 & 0 \\ \delta/2 & 0 & 0 \\ 0 & 0 & 0 \end{pmatrix} \quad (3)$$

where the indices are given in Voigt notation. Sufficiently small strains of  $\delta = \pm 0.5\%$  were applied, and elastic coefficients were obtained by averaging stresses from positive and negative strains. Table 3 summarizes the computed elastic coefficients from using LDA and GGA exchange-correlation functionals.

Adiabatic mechanical constants can be derived from the computed elastic constants [29]. The bound values were computed using elastic coefficients,  $C$ , determined from Eqn. (2). From the computed  $K_{RVH}$  and  $G_{RVH}$ , the Young's modulus ( $E$ ) and Poisson ratio ( $\eta$ ) were calculated. The computed RVH mechanical properties are summarized in Table 3. Furthermore, the Young's modulus for uniaxial compression along arbitrary directions was computed. The definition of the directional Young's modulus can be found in previous work on crystalline calcium silicate hydrate [30]. Calculated magnitudes of the LDA and GGA Young's modulus are

**Table 3**  
Calculated elastic coefficients (GPa) and RVH based averaged mechanical properties.

	DFT_GGA	DFT_LDA		DFT_GGA	DFT_LDA
$C_{11}$	<b>57.1</b>	91.2	K (GPa)	<b>32(1)</b>	48(2)
$C_{12}$	<b>16.5</b>	24.7	G (GPa)	<b>24(1)</b>	31(1)
$C_{13}$	<b>5.7</b>	21.2	E (GPa)	<b>59</b>	77
$C_{22}$	<b>61.0</b>	67.9	$\eta$	<b>0.2</b>	0.2
$C_{23}$	<b>15.1</b>	30.4			
$C_{33}$	<b>103.7</b>	135.8			
$C_{44}$	<b>18.4</b>	23.3			
$C_{55}$	<b>20.7</b>	25.8			
$C_{66}$	<b>26.8</b>	42.6			

Note: Reliable predictions (GGA) are in bold. Isothermal bulk modulus ( $K_0$ ) from HPXRD is 30(4) GPa.

represented in colors on the surface of the sphere. The  $X$ ,  $Y$ , and  $Z$  directions shown in Fig. 7 are defined in  $([fx], \vec{Z} \parallel \vec{a} \times \vec{b}, \text{ and } \vec{Y} \parallel \vec{Z} \times \vec{X})$  setting [31].

#### 4. Discussion

The measured XRD pattern at ambient condition without the DAC (i.e., peak at 0 GPa) matches well with published reference peaks [9]. It was previously reported that it was difficult to synthesize kanemite with a high crystallinity that was characterized by lab-based XRD [32]. In current study, high-energy source XRD provides an enough resolution to identify the obtained crystallinity from the synthesized sample. Under applied pressures with the DAC, XRD peaks tend to generally diffuse especially for layered minerals containing with hydrogens or water molecules [14]. Along with this usual phenomenon, the 020 interlayer peak was becoming disappeared as pressure increased. It indicates the collapse of layer structure under pressure. In cases of some calcium aluminate hydrates that can hold several interlayer molecules, it was reported that pressure-induced dehydration may occur at low hydrostatic pressure [14]. Water molecules in interlayer region could move out from the calcium aluminate structure under certain low pressure. It causes stepwise shrinkage of layer spacing and makes the crystal mechanically more incompressible. The phenomenon was previously confirmed by testing two different types of pressure-transmitting media of hygroscopic and non-hygroscopic. With hygroscopic solution, it absorbed water molecules coming from interlayer and the shrinkage behavior was not reversible. On the other hand, the dehydration effect was reversible with the non-hygroscopic solution [14,33].

In current study, the weakened interlayer peak of 020 was reappeared when the applied pressure was released from 3 to 0.1 GPa. This experimental observation suggests that this phase instability of Na-kanemite is reversible with the non-hygroscopic solution (i.e., silicone oil) although the reflection intensity of reappeared interlayer peak is weakened. Furthermore, a new peak around 6.8 Å that also moved under higher pressures, was observed. Since it shows normal behavior under pressure, it should come from the sample in the DAC. Considering the position of the peak (i.e., 6.8 Å), it can be inferred that the hidden 011 peak in  $Pbcn$  symmetry appeared under pressure due to the reduction of symmetry to  $P1c1$  or eventually to  $P11n$ . Upon unloading, the new 011 peak disappeared as the interlayer 020 peak reappeared. It again confirms that this transformation is reversible. Similarly, temperature-dependent dehydration of kanemite was reported

[32]. At temperature of 60 and 150 °C, it was dehydrated to  $\text{NaSi}_2\text{O}_4(\text{OH}) \cdot \text{H}_2\text{O}$  (monohydrate) and  $\text{NaSi}_2\text{O}_4(\text{OH})$ , respectively. In this case of temperature-induced dehydration, detail crystallographic data was resolved for the two dehydration steps. However, for this study of pressure-induced reaction, further structural investigation is needed to refine the detail atomic information of this temporal phase transition which was not able to be achieved due to the small amount of tested sample, weakened peak intensities under pressures, and additional peaks from the DAC and ruby chips. Another observation from the HPXRD is as follows. While lattice parameters of  $a$  and  $b$  show stable pressure behavior (Table 2 and Figs. 3 and 4), lattice parameter  $c$  shows non-linear behavior. It could be interpreted by having one abnormal data point at 1.5 GPa (i.e., potential error of pressure measurement) or due to the amorphization of layer and/or the formation of the new peak that was not considered during the refinement of lattice parameters. However, the ruby fluorescence measurement was relatively accurate as indicated by small standard deviations of calibrated pressures in Figs. 3–6. On the other hand, it was previously reported that the stability and crystallinity of kanemite depend on the water content [9]. During potential dehydration process under pressure, poor crystallinity and stacking disorder may affect the refinement accuracy. In current experiment, it is concluded that less crystallinity and reversible symmetry reduction upon pressurization resulted in the slightly abnormal data point rather than measurement error of pressure.

First-principles calculation provides accurate atomic level movement of crystals under pressure that is usefully combined with HPXRD experiments [31,34]. Because of the high accuracy, it is being intensively used to predict or simulate phase transition under pressure [35]. In current study, although there are some experimental observations indicating potential phase instability of Na-kanemite (i.e., the diffused 020 interlayer peak and new 011 peak formation), anomalous pressure behavior was not captured from conducted calculations. The optimized crystallographic data from two different functionals of LDA and GGA are compared in Table 2. Using GGA functional, there is an excellent agreement of the pressure-volume behavior of Na-kanemite from HPXRD and first-principles calculation (Fig. 6). On the other hand, the pressure-trajectories of three lattice parameters predicted from the GGA functional are quite different. It underestimates the lattice parameters of  $a$  and  $c$  while it overestimates that of  $b$  under pressures (Figs. 3–5). In overall, they compensate for each other, providing a good agreement of the pressure-volume behavior of Na-kanemite when the GGA functional is used (Fig. 6). However, LDA

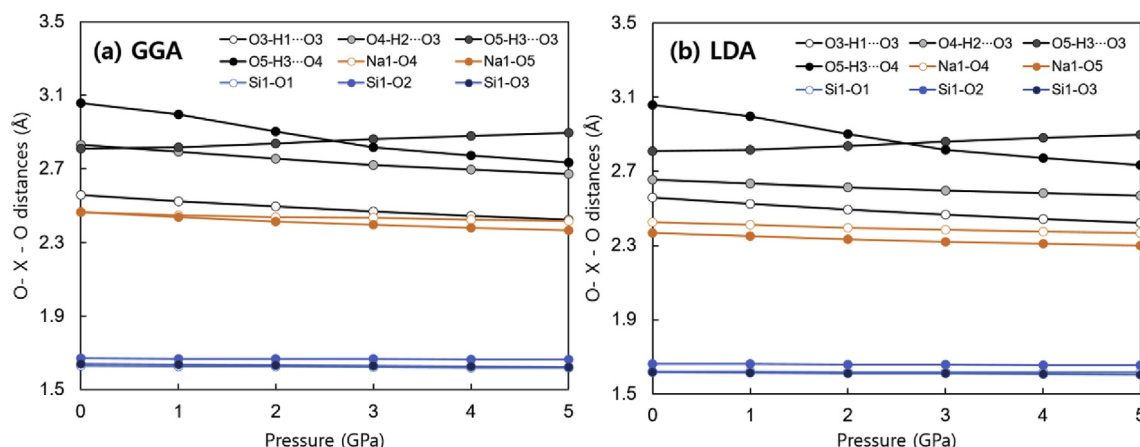


Fig. 7. Variation of O – X – O bond distances under pressure from GGA (a) and LDA (b) calculations.

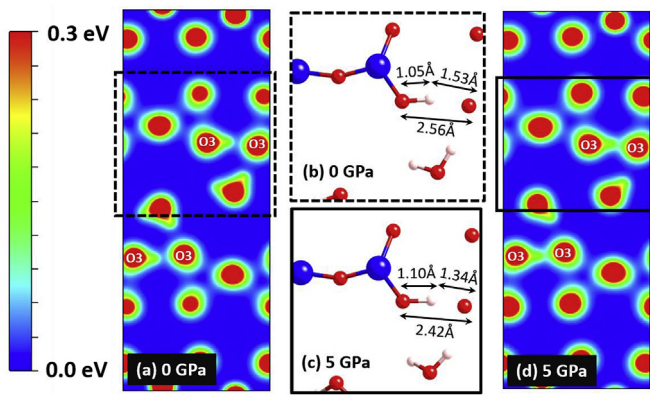


Fig. 8. Pressure induced variations of charge distribution and bond length at 0 GPa (a and b) and 5 GPa (c and d).

underestimates the lattice parameter  $a$  quite significantly whereas data points of  $b$  and  $c$  are in the range of experimental points (Figs. 3–5). It results in the discrepancy of  $P$ – $V$  data (Fig. 6).

In previous study on hydrated minerals of calcium aluminate hydrate and calcium silicate hydrate, there is an excellent agreement between LDA with that from HPXRD regarding pressure-volume behavior and resulting mechanical responses [30,31]. Using GGA functional, first-principles calculations overestimate volumes under pressure that results in lower mechanical properties. In the case of Na-kanemite, the conducted first-principle calculation does not show any phase instability under pressure in the investigated pressure range of 0–5 GPa. This indicates that instability or temporal phase transition during HPXRD experiment may be related with external environment, for instance, from the extrinsic effect from the use of pressure-transmitting medium or interplay between the medium and Na-kanemite. In addition, the experimental phenomena can be due to the effect of van der Waals dispersion or vibration from water molecules in the interlayer region as these have been disregarded in conducted static calculations.

Variation of bond distances of Si–O, Na–O, and O–O in O–H...O under pressure, was analyzed to examine the pressure absorbance of silicate layer, Na layer, and space between the two layers, respectively (Fig. 7). In general, the distances decreased as the pressure increases except O5–H3...O4 bond. In addition, the degree of reduction of O5–H3...O3 bond is more significant than the others. These can be explained by the contraction of thickness and the distortion of Na layer upon pressurization. The reduction rate of other bonds is lower in the order of O–H...O, Na–O and Si–O,

confirming that the order of pressure absorbance is space between silicate and Na layers, Na layer, and silicate layer, respectively.

Fig. 8 shows conducted Bader charge analysis to understand the detail binding force at zero pressure and 5 GPa based on GGA functional calculation [36]. Partial charge which can be related to the binding force, was obtained by subtracting the number of valence electrons from the computed Bader charge. At zero pressure, some O3 atoms without H cation have an average partial charge of  $-1.76$  eV while the other O3 with H cation have the value of  $-2.03$  eV. Under pressure of 5 GPa, each partial charge values decreased to  $-1.72$  eV ( $-2.30\%$ ) and increased to  $-2.05$  eV ( $1.17\%$ ), respectively (Fig. 9). As can be confirmed by charge distribution plot of Fig. 8, the bond distance between O3–H5 increased from  $1.05$  Å to  $1.10$  Å even under pressure of 5 GPa. It can be inferred that the Bader volume of O3 without hydrogen atoms decreased dominantly under pressure whereas that of O3 with hydrogen atoms increased. This phenomenon can be also confirmed by the conducted charge analysis that indicates the preference of charge redistribution under pressure (Fig. 9).

The computational reliability of first-principles calculations highly depends on the ability of the exchange-correlation functional to mimic many-body electronic interactions in a system. Thus there is a tendency of general underestimation of lattice parameter and resulting overestimation of elastic constants, and vice versa. As a result of potential complicated effects to influence the atomic responses, the HPXRD experiment provides the bulk modulus of 30(4) based on the obtained  $P$ – $V$  data points. From the achieved good agreement of bulk modulus (i.e., 32(1) GPa from RVH and 30(4) from HPXRD, Table 3), it can be suggested that computed elastic constants and mechanical properties from the GGA functional are more reliable. The more reliable data is summarized in Table 3.

Fig. 10(a) and (b) show directional Young's modulus measured from GGA and LDA functionals, respectively. At zero pressure, large structural anisotropy of Na-kanemite that is commonly found in layered minerals, is evident. The most compressible direction is perpendicular to the layer which is more clearly observed with LDA functional (Fig. 10). Previously, it was reported that ASR gel has an isothermal bulk modulus of 33(2) GPa [37]. The measurement of amorphous material was performed based on x-ray absorption experiment under various uniaxial pressures. Current study suggests similar bulk modulus of Na-kanemite as  $K_0$  is  $30 \pm 4$  GPa. This similarity of bulk modulus of crystalline Na-kanemite and amorphous ASR gel may be due to the pressure induced dehydration (or amorphization) in the Na-kanemite, which is observed in current HPXRD study. In other words, similar to a gel material that does not have distinct layers, the layer of Na-kanemite may tend to easily

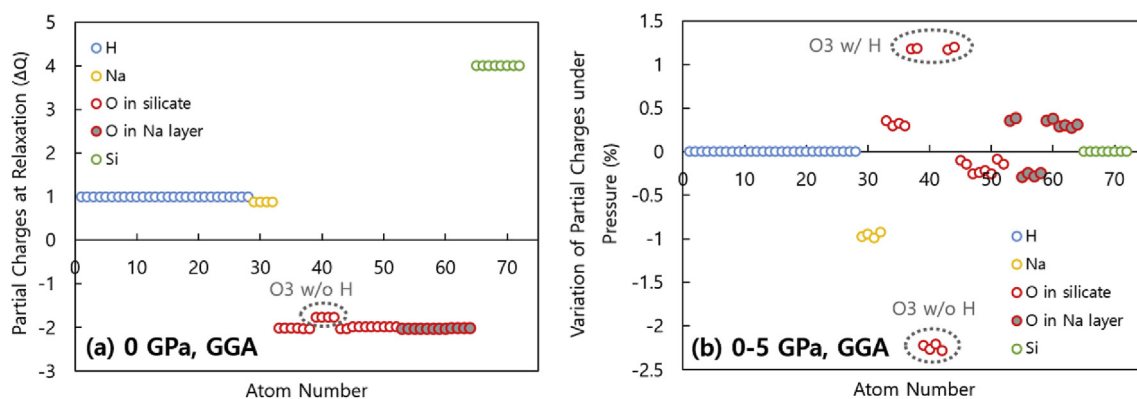
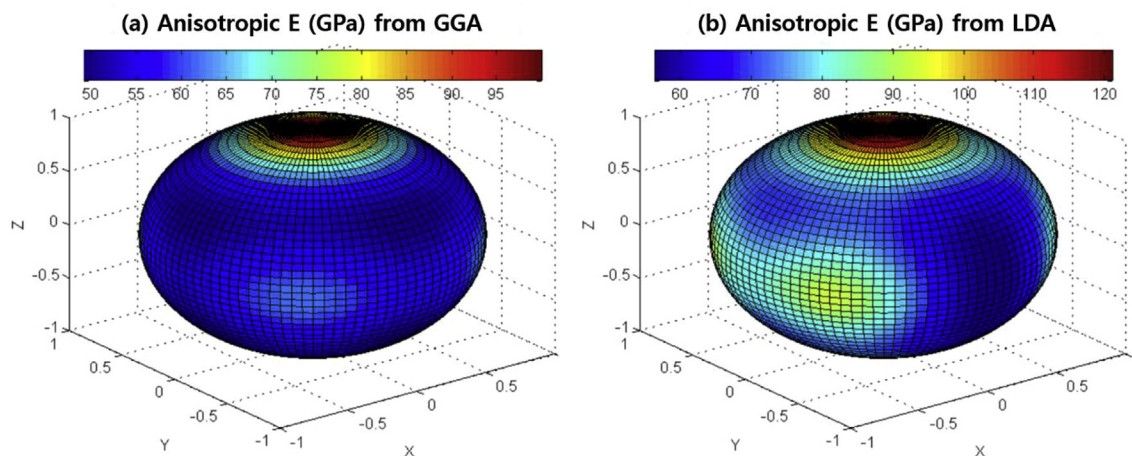


Fig. 9. Bader charge analysis based on GGA calculation at 0 GPa (a) and its variation (%) due to pressurization of 5 GPa (b).



**Fig. 10.** Computed directional Young's modulus using (a) GGA and (b) LDA functionals in the crystallographic setting of  $\vec{X} \parallel \vec{a}$ ,  $\vec{Z} \parallel \vec{a} \times \vec{b}$ , and  $\vec{Y} \parallel \vec{Z} \times \vec{X}$ ,  $\vec{Z} \parallel \vec{a}$ ,  $\vec{X} \parallel \vec{a} \times \vec{b}$ , and  $\vec{Y} \parallel \vec{Z} \times \vec{X}$ . Scale bars indicate Young's modulus in GPa.

collapse under low pressure. Because the mechanical property obtained from HXPRD experiment is the averaged bulk modulus in the range of 0–5 GPa, it is possible that it has similar bulk modulus with ASR gel due to the early collapse of layer structure. Furthermore, the two dehydration steps of kanemite were experimentally confirmed upon the temperature of 60 and 150 °C, recently [32]. Increasing hydrogen bonding between layers causes dehydration reaction which involves interlayer peak diffusion and new peak formation around 7 Å. It is interesting to note that the new peak formed at similar position which observed during HPXRD experiment (Fig. 2). So it can be an indirect evidence to support that the temporal and reversible phase instability under pressure can be a reversible dehydration reaction with increasing hydrogen bonding between layers and caused the symmetry reduction of *Pbcn*.

## 5. Conclusions

The conducted study expands previous investigations of temperature-induced dehydration of kanemite. For the first time, it was confirmed that possible dehydration occurred under low hydrostatic pressure of 0.4 GPa. Similar with the temperature-induced dehydration, a new formation of 110 peak indicates the potential symmetry reduction of *Pncn* to *P1c1* or *P11n*. The transformation was reversible but rehydration observed with a loss of crystallinity of the sample. Thus, detail structural information was not successfully obtained due to the diffused peaks and the fact that XRD is not able to identify H positions.

However, computational analysis revealed that applied pressure was absorbed by the order of space between silicate and Na layers, Na layer, and silicate layer. Lastly, reliable mechanical properties and elastic constants of Na-kanemite could be proposed based on the good agreement between HPXRD at low pressure and first-principles calculations. This accurately confirmed elastic properties and conducted Bader charge data will be used to validate existing potentials or develop more advanced force-field database such as ClayFF or cemFF to simulate large-scale molecular dynamics of cementitious materials and clay-like minerals and to serve a database to design infrastructure more robust especially against ASR [38,39].

## Data availability

The raw/processed data required to reproduce these finding can be shared upon the request to the corresponding author.

## CRedit authorship contribution statement

**Juhyuk Moon:** Conceptualization, Data curation, Funding acquisition, Investigation, Writing - original draft, Writing - review & editing. **Seungchan Kim:** Formal analysis, Investigation, Methodology, Visualization. **Cagla Meral Akgul:** Formal analysis, Investigation. **Sung-Chul Bae:** Formal analysis, Investigation. **Simon Martin Clark:** Conceptualization, Validation, Writing - review & editing.

## Acknowledgements

This publication was supported by the Basic Science Research Program through the National Research Foundation of Korea (NRF) funded by the Ministry of Education, Republic of Korea (NRF-2018R1C1B6003058). The Institute of Engineering Research in Seoul National University provided research facilities for this work.

## References

- [1] C. Hu, Y. Gao, B. Chen, Y. Zhang, Z. Li, Estimation of the poroelastic properties of calcium-silicate-hydrate (CSH) gel, *Mater. Des.* 92 (2016) 107.
- [2] E. Sassoni, G. Graziani, G. Ridolfi, M.C. Bignozzi, E. Franzoni, Thermal behavior of Carrara marble after consolidation by ammonium phosphate, ammonium oxalate and ethyl silicate, *Mater. Des.* 120 (2017) 345.
- [3] Y.-r. Yang, Q.-j. Zhang, W. Cai, M.-g. Yi, L. Xiang, Formation and application of hierarchical calcium silicate-calcium sulfate whiskers, *Mater. Des.* 146 (2018) 172.
- [4] A. Kalt, R. Wey, Composés interfoliaires d'une silice hydratée cristallisée, *Bull. Groupe Fr. Des. Argiles* 20 (2) (1968) 205.
- [5] Z. Johan, G. Maglione, Kanemite, a new hydrated sodium silicate, *Bull. Soc. Fr. Mineral. Cristallogr.* 95 (3) (1972) 371.
- [6] K.-F. Hesse, F. Liebau, Crystal chemistry of silica-rich Barium silicates, *Z. für Kristallogr. - Cryst. Mater.* 153 (1–4) (1980) 3.
- [7] G.G. Almond, R.K. Harris, K.R. Franklin, A structural consideration of kanemite, octosilicate, magadiite and kenyaite, *J. Mater. Chem.* 7 (4) (1997) 681.
- [8] S. Hayashi, Solid-state NMR study of locations and dynamics of interlayer water in kanemite, *J. Mater. Chem.* 7 (6) (1997) 1043.
- [9] S. Vortmann, J. Rius, B. Marler, H. Gies, Structure solution from powder data of the hydrous layer silicate kanemite, a precursor of the industrial ion exchanger SKS-6, *Eur. J. Mineral.* (1999) 125.
- [10] L.A. Garvie, B. Devouard, T.L. Groy, F. Cámara, P.R. Buseck, Crystal structure of kanemite,  $\text{NaHSi}_2\text{O}_5 \cdot 3\text{H}_2\text{O}$ , from the Aris phonolite, Namibia, *Am. Mineral.* 84 (7–8) (1999) 1170.
- [11] Y. Li, X. Cheng, W. Cao, L. Gong, R. Zhang, H. Zhang, Fabrication of adiabatic foam at low temperature with sodium silicate as raw material, *Mater. Des.* 88 (2015) 1008.
- [12] R. Kirkpatrick, A. Kalinichev, X. Hou, L. Struble, Experimental and molecular dynamics modeling studies of interlayer swelling: water incorporation in kanemite and ASR gel, *Mater. Struct.* 38 (4) (2005) 449.
- [13] Z. Shi, G. Geng, A. Leemann, B. Lothenbach, Synthesis, characterization, and

- water uptake property of alkali-silica reaction products, *Cement Concr. Res.* 121 (2019) 58.
- [14] J.-h. Moon, J.E. Oh, M. Balonis, F.P. Glasser, S.M. Clark, P.J. Monteiro, Pressure induced reactions amongst calcium aluminate hydrate phases, *Cement Concr. Res.* 41 (6) (2011) 571.
- [15] A. Cuesta, P. Rejmak, A. Ayuela, A. De la Torre, I. Santacruz, L. Carrasco, C. Popescu, M. Aranda, Experimental and theoretical high pressure study of calcium hydroxyaluminate phases, *Cement Concr. Res.* 97 (2017) 1.
- [16] G. Geng, R.J. Myers, M.J.A. Qomi, P.J. Monteiro, Densification of the interlayer spacing governs the nanomechanical properties of calcium-silicate-hydrate, *Sci. Rep.* 7 (1) (2017) 10986.
- [17] G. Geng, R.N. Vasin, J. Li, M.J.A. Qomi, J. Yan, H.-R. Wenk, P.J. Monteiro, Preferred orientation of calcium aluminosilicate hydrate induced by confined compression, *Cement Concr. Res.* 113 (2018) 186.
- [18] B.-X. Dong, H.-Y. Yang, F. Qiu, Q. Li, S.-L. Shu, B.-Q. Zhang, Q.-C. Jiang, Design of TiCx Nanoparticles and Their Morphology Manipulating Mechanisms by Stoichiometric Ratios: Experiment and First-Principle Calculation, *Materials & Design*, 2019, p. 107951.
- [19] O. Khyzhun, V. Bekenev, V. Atuchin, L. Pokrovsky, V. Shlegel, N. Ivannikova, The electronic structure of Pb<sub>2</sub>MoO<sub>5</sub>: first-principles DFT calculations and X-ray spectroscopy measurements, *Mater. Des.* 105 (2016) 315.
- [20] K. Beneke, G. Lagaly, Kanemite; innercrystalline reactivity and relations to other sodium silicates, *Am. Mineral.* 62 (7–8) (1977) 763.
- [21] M. Kunz, A.A. MacDowell, W.A. Caldwell, D. Cambie, R.S. Celestre, E.E. Domning, R.M. Duarte, A.E. Gleason, J.M. Glossinger, N. Kelez, A beamline for high-pressure studies at the Advanced Light Source with a superconducting bending magnet as the source, *J. Synchrotron Radiat.* 12 (5) (2005) 650.
- [22] H. Mao, J.-A. Xu, P. Bell, Calibration of the ruby pressure gauge to 800 kbar under quasi-hydrostatic conditions, *J. Geophys. Res.: Solid Earth* 91 (B5) (1986) 4673.
- [23] A. Hammersley, S. Svensson, M. Hanfland, A. Fitch, D. Hausermann, Two-dimensional detector software: from real detector to idealised image or two-theta scan, *Int. J. High Press. Res.* 14 (4–6) (1996) 235.
- [24] J. Laugier, B. Bochu, CELREF: Cell Parameters Refinement Program from Powder Diffraction Diagram, Laboratoire des Matériaux et du Génie Physique, Ecole Nationale Supérieure de Physique de Grenoble (INPG), Grenoble, France, 1999.
- [25] F. Birch, Finite strain isotherm and velocities for single-crystal and polycrystalline NaCl at high pressures and 300 K, *J. Geophys. Res.* 83 (B3) (1978) 1257.
- [26] G. Paolo, et al., Quantum ESPRESSO: a modular and open-source software project for quantum simulations of materials, *J. Phys. Condens. Matter* 21 (39) (2009) 395502.
- [27] H.J. Monkhorst, J.D. Pack, Special points for Brillouin-zone integrations, *Phys. Rev. B* 13 (12) (1976) 5188.
- [28] R.M. Wentzcovitch, Invariant molecular-dynamics approach to structural phase transitions, *Phys. Rev. B* 44 (5) (1991) 2358.
- [29] R. Hill, The elastic behaviour of a crystalline aggregate, *Proc. Phys. Soc. Sect. A* 65 (5) (1952).
- [30] J. Moon, S. Yoon, P.J. Monteiro, Mechanical properties of jennite: a theoretical and experimental study, *Cement Concr. Res.* 71 (2015) 106.
- [31] J. Moon, S. Yoon, R.M. Wentzcovitch, P.J. Monteiro, First-principles elasticity of monocarboaluminate hydrates, *Am. Mineral.* 99 (7) (2014) 1360.
- [32] D. Schmidmair, V. Kahlenberg, D.M. Töbrens, H. Schottenberger, J. De Wit, U.J. Griesser, Temperature- and moisture-dependent powder X-ray diffraction studies of kanemite (NaSi<sub>2</sub>O<sub>4</sub>(OH)·3H<sub>2</sub>O), *Mineral. Mag.* 79 (1) (2015) 103.
- [33] J. Moon, J. Oh, M. Balonis, F.P. Glasser, S.M. Clark, P.J.M. Monteiro, High pressure study of low compressibility tetracalcium aluminum carbonate hydrates 3CaO·Al<sub>2</sub>O<sub>3</sub>·CaCO<sub>3</sub>·11H<sub>2</sub>O, *Cement Concr. Res.* 42 (1) (2012) 105.
- [34] J. Moon, S. Yoon, R.M. Wentzcovitch, S.M. Clark, P.J. Monteiro, Elastic properties of tricalcium aluminate from high-pressure experiments and first-principles calculations, *J. Am. Ceram. Soc.* 95 (9) (2012) 2972.
- [35] T. Tsuchiya, J. Tsuchiya, K. Umamoto, R.M. Wentzcovitch, Phase transition in MgSiO<sub>3</sub> perovskite in the Earth's lower mantle, *Earth Planet. Sci. Lett.* 224 (3) (2004) 241.
- [36] R.F. Bader, R. F. Atoms in molecules, *Accounts of Chemical Research* 18 (1) (1985) 9.
- [37] J. Moon, S. Speziale, C. Meral, B. Kalkan, S.M. Clark, P.J.M. Monteiro, Determination of the elastic properties of amorphous materials: case study of alkali-silica reaction gel, *Cement Concr. Res.* 54 (2013) 55.
- [38] R.T. Cygan, J.-J. Liang, A.G. Kalinichev, Molecular models of hydroxide, oxyhydroxide, and clay phases and the development of a general force field, *J. Phys. Chem. B* 108 (4) (2004) 1255.
- [39] R.K. Mishra, A.K. Mohamed, D. Geissbühler, H. Manzano, T. Jamil, R. Shahsavari, A.G. Kalinichev, S. Galmarini, L. Tao, H. Heinz, cemff, A force field database for cementitious materials including validations, applications and opportunities, *Cement Concr. Res.* 102 (2017) 68.